Solid Freeform Fabrication 2019: Proceedings of the 30th Annual International
Solid Freeform Fabrication Symposium – An Additive Manufacturing Conference
Reviewed Paper

AN ALUMINUM-LITHIUM ALLOY PRODUCED BY LASER POWDER BED FUSION

Yang Qi*, Hu Zhang†, Haihong Zhu*, Xiaojia Nie*, Xiaoyan Zeng*
*Wuhan National Laboratory for Optoelectronics, Huazhong University of Science and Technology, Wuhan, Hubei 430074, PR China
†School of Optical and Electronic Information, Huazhong University of Science and Technology, Wuhan, Hubei 430074, PR China

Abstract

Aluminum-lithium (Al-Li) alloys are promising to replace traditional high-strength aluminum alloys in aerospace and military industries due to their low density, high specific strength, and excellent corrosion resistance. However, there is little research focused on the laser powder bed fusion (LPBF) of Al-Li alloys due to their poor weldability and high crack susceptibility. In this study, the feasibility of the Al-Li alloy fabricated by LPBF was investigated. The effect of the processing parameters on the densification and crack formation behavior was studied. Finally, after optimizing the processing parameters, crack-free and nearly fully dense 2195 Al-Li alloy 3D-printed samples were obtained. A relative density of 99.92% and a microhardness of 89.1 HV were achieved.

Introduction

Aluminum-lithium (Al-Li) alloys are of great interest to the aerospace and military industries because they offer many advantages over conventional aluminum alloys [1]. Their low density, high specific strength, and excellent corrosion resistance can bring significant weight savings [2], leading to Al-Li alloys being increasingly substituted for conventional 2xxx and 7xxx series high-strength aluminum alloys [3]. The 2195 Al-Cu-Li-Mg-Ag alloy, one of the representative latest generation of aluminum-lithium alloys, has been used in the production of the lightweight parts in aerospace [4], due to its excellent strength at room temperature [5] and high performance even at cryogenic atmosphere [6].

However, the traditional manufacturing methods of Al-Li alloys, including casting, pressing, and extrusion are complex, time-consuming and unable to produce complex structures [7]. The laser powder bed fusion (LPBF), also known as selective laser melting, is an additive manufacturing technology with design freedom and manufacturing flexibility. The LPBF has the advantages of short cycle times, low tooling costs, and eliminating consumption-of-scale constraints [8][9]. Nowadays, the printable materials of the LPBF are focused on the steel [10][11], nickel-based superalloy [12][13], titanium alloy [14][15], and aluminum-silicon alloy [16][17]. The 2xxx and 7xxx series high-strength aluminum alloys with poor weldability have also been reported to be successfully fabricated by the LPBF [18][19][20][21][22]. Little research is focused on the LPBF of Al-Li alloys till now. Al-Li alloys are susceptible to hot cracking during laser processing due to their high coefficient of thermal expansion and eutectics formation during solidification [23].

This work investigated the feasibility of the 2195 Al-Li alloy fabricated by LPBF. The effect of the scanning velocity, hatch spacing, and the volumetric energy density on the densification and crack formation behavior was studied.

Materials and methods

Gas-atomized 2195 Al-Li powders supplied by Intelligence Manufacturing Technology were used in this study. The chemical composition listed in Table 1 was analyzed by Inductively Coupled Plasma Optical Emission Spectrometry (ICP-OES). The powder morphology was observed by an FEI Nova Nano SEM 450 scanning electron microscope (SEM) as shown in Fig. 1a. The raw powder consists of many spherical powder particles and some small aggregated satellite particles attached to the big particles. The powder particle size distribution shown in Fig. 1b was measured by Malvern UK Mastersizer 3000.

Table 1. Chemical composition (wt.%) of the powder used in this study

Element	Cu	Li	Mg	Ag	Zr	Si	Al
Powder	3.95	1.08	0.68	0.40	0.11	0.05	Bal.

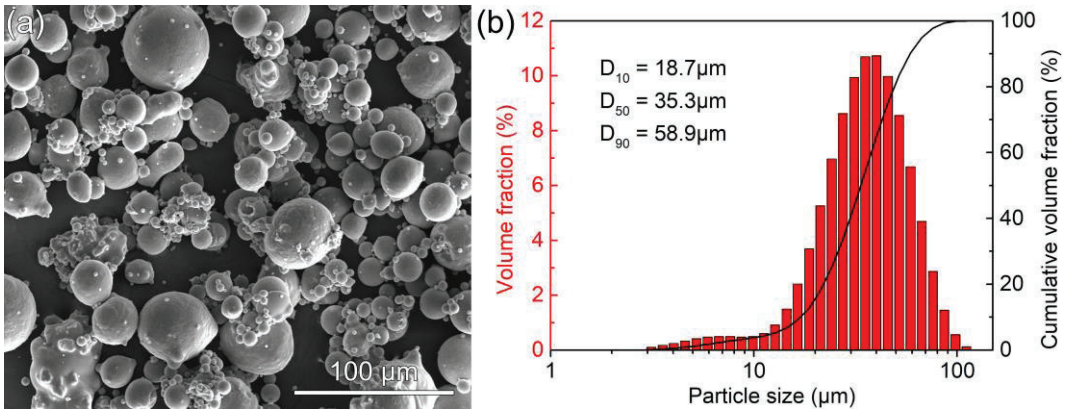

Fig. 1. (a) SEM image showing the morphology of the raw powder. (b) Powder particle size distribution.

The LPBF experiment was carried out at room temperature on a self-developed LPBF machine (LSNF-I). The LPBF machine consists of a continuous wave IPG YLR-200 fiber laser with a maximum laser power of 200W, and other details have been given elsewhere [24][25]. All samples were fabricated under a protective argon atmosphere with the concentrations of H_2O and O_2 controlled below 100 ppm. To investigate the feasibility of the Al-Li alloy fabricated by LPBF, 8 mm (length) × 8 mm (width) × 4 mm (height) cubic samples were built with different processing parameters. The laser power, layer thickness, and the layer-to-layer rotation angle were fixed at 200 W, 30 μm, and 90°, respectively. Other processing parameters are shown in Table 2.

Table 2. LPBF processing parameters used in this study

Parameters (Unit)	Value
Scanning velocity (mm/s)	80, 160, 240, and 320
Hatch spacing (mm)	0.06, 0.08, 0.10, and 0.12

The relative density of every cubic sample was obtained by image processing of six optical microscope graphs using Image-Pro Plus 6.0 software. All samples were subjected to a standard metallographic procedure.

Results and discussions

Fig. 2 shows the effect of the scanning velocity on the relative density with a fixed hatch spacing of 0.12 mm. The relative density decreases as the scanning velocity increases. For every 80 mm/s increase in the scanning velocity, the relative density decreases more. The nearly fully dense 2195 Al-Li alloy sample is obtained when the scanning velocity is 80 mm/s.

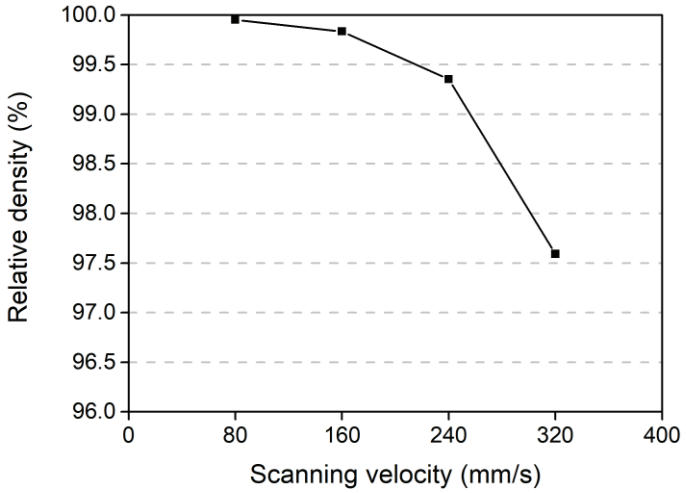

Fig. 2. Effect of the scanning velocity on the relative density.

Fig. 3 presents the optical microscope graphs of polished samples fabricated with different scanning velocity at a fixed hatch spacing of 0.12 mm. The irregular pores are found to be in all the samples, and the size of the irregular pores increases with the increase of the scanning velocity. The cracks begin to appear when the scanning velocity is 160 mm/s, and the amount of the cracks tends to increase with the increase of the scanning velocity.

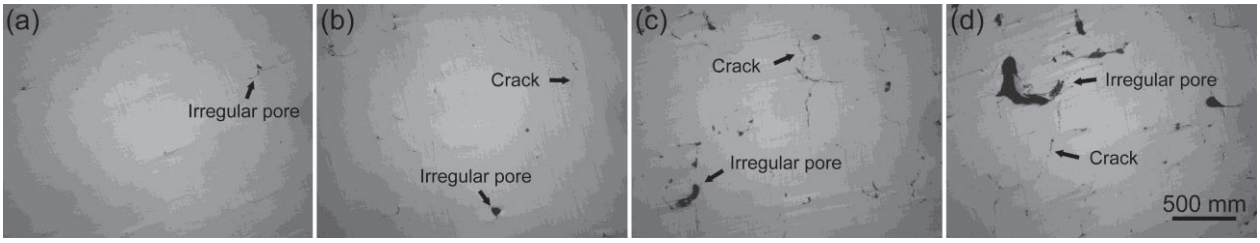

Fig. 3. Optical microscope graphs of polished samples fabricated at a fixed hatch spacing of 0.12 mm with different scanning velocity: (a) 80 mm/s, (b) 160 mm/s, (c) 240 mm/s, (d) 320 mm/s.

To further study the effect of the hatch spacing on the relative density and the crack formation, Fig. 4 shows the effect of the hatch spacing on the relative density with a scanning velocity of 160 mm/s. The relative density of all the samples is above 99.8%, indicating that decreasing the hatch spacing has little effect on the relative density.

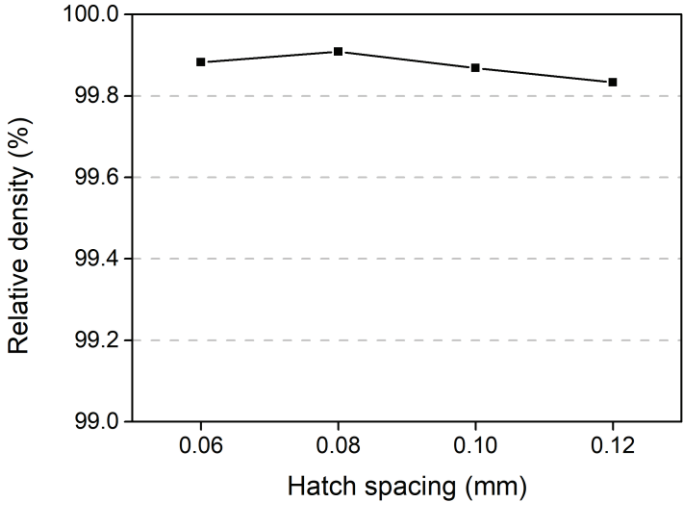

Fig. 4. Effect of the hatch spacing on the relative density.

Fig. 5 presents the optical microscope graphs of polished samples fabricated with different hatch spacing at a fixed scanning velocity of 160 mm/s. When the hatch spacing is smaller than 0.10 mm, the cracks are absent. So decreasing the hatch spacing is beneficial to eliminate cracks.

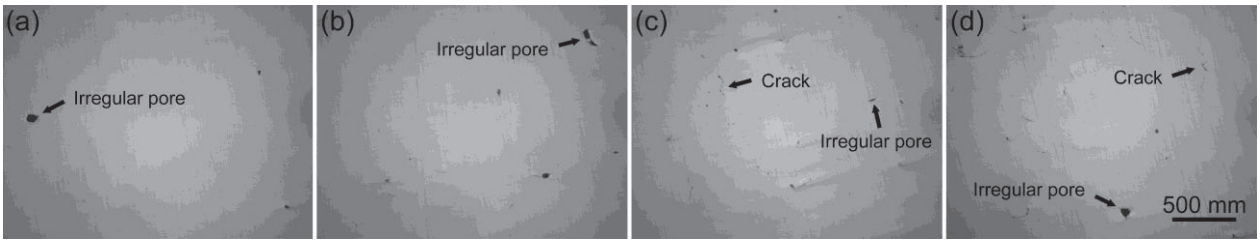

Fig. 5. Optical microscope graphs of polished samples fabricated at a fixed scanning velocity of 160 mm/s with different hatch spacing: (a) 0.06 mm, (b) 0.08 mm, (c) 0.10 mm, (d) 0.12 mm.

To comprehensively consider the effect of various processing parameters on the densification and crack formation behavior, the volumetric energy density (VED) is induced and given by:

$$\mathrm{VED} = \frac{P}{V \cdot H \cdot T}$$

where P is the laser power, V is the laser scanning velocity (mm/s), H is the hatch spacing (mm), T is the layer thickness (μm).

Fig. 6 shows the effect of the volumetric energy density on the relative density and crack formation. Processing at similar volumetric energy density leads to variations of the relative density, indicating that the volumetric energy density is not a very reliable parameter for predicting the relative density, as reported by Prashanth et al. [26]. When the volumetric energy density is larger than 520 J/mm^3, cracks are difficult to be found in the optical microscope graphs of the samples. As the volumetric energy density is positively correlated with the temperature in the molten zone, the high volumetric energy density leads to a long lifetime of the molten pool, then reduces the crack susceptibility.

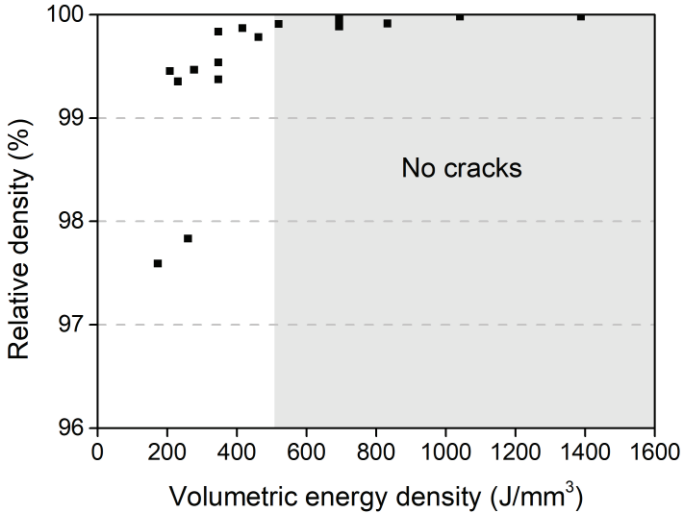

Fig. 6. Effect of the volumetric energy density on the relative density and the crack formation

Considering the porosity and the fabricating efficiency, the optimized parameters are the laser power of 200 W, the layer thickness of 30 μm, the scanning velocity of 80 mm/s, and the hatch spacing of 0.1 mm. The relative density and the microhardness of the sample built with the optimized parameters are 99.92% and 89.1 HV respectively.

Conclusions

The feasibility of the 2195 Al-Li alloy fabricated by LPBF has been successfully proved. The sample fabricated with the optimized parameters is crack-free and nearly fully dense with a relative density of 99.92% and a microhardness of 89.1 HV. The volumetric energy density is crucial for determining the crack formation. Crack-free samples can be obtained when the volumetric energy density is above 520 J/mm^3.

Future works

Future works will focus on the tensile performance and the heat treatment of the 2195 Al-Li alloy fabricated by LPBF.

Acknowledgments

This work was supported by the National Natural Science Foundation of China (Grant No. 51805184). The authors would also like to thank the Analytical and Testing Center of HUST for the SEM analysis.

References

[1] R.J. Rioja, J. Liu, The Evolution of Al-Li Base Products for Aerospace and Space Applications, Metall. Mater. Trans. A. 43 (2012) 3325–3337. doi:10.1007/s11661-012-1155-z.

[2] T. Dursun, C. Soutis, Recent developments in advanced aircraft aluminium alloys, Mater. Des. 56 (2014) 862–871. doi:10.1016/j.matdes.2013.12.002.

[3] B.I. Rodgers, P.B. Prangnell, Quantification of the influence of increased pre-stretching on microstructure-strength relationships in the Al–Cu–Li alloy AA2195, Acta Mater. 108 (2016) 55–67. doi:10.1016/j.actamat.2016.02.017.
[4] J.-H. Kim, J.-H. Jeun, H.-J. Chun, Y.R. Lee, J.-T. Yoo, J.-H. Yoon, H.-S. Lee, Effect of precipitates on mechanical properties of AA2195, J. Alloys Compd. 669 (2016) 187–198. doi:10.1016/j.jallcom.2016.01.229.
[5] Y. Wang, G. Zhao, X. Xu, X. Chen, W. Zhang, Microstructures and mechanical properties of spray deposited 2195 Al-Cu-Li alloy through thermo-mechanical processing, Mater. Sci. Eng. A. 727 (2018) 78–89. doi:10.1016/j.msea.2018.04.116.
[6] N. Nayan, S.V.S. Narayana Murty, A.K. Jha, B. Pant, S.C. Sharma, K.M. George, G.V.S. Sastry, Mechanical properties of aluminium-copper-lithium alloy AA2195 at cryogenic temperatures, Mater. Des. 58 (2014) 445–450. doi:10.1016/j.matdes.2014.02.024.
[7] T.B. Sercombe, Rapid Manufacturing of Aluminum Components, Science (80-.). 301 (2003) 1225–1227. doi:10.1126/science.1086989.
[8] J.H. Martin, B.D. Yahata, J.M. Hundley, J.A. Mayer, T.A. Schaedler, T.M. Pollock, 3D printing of high-strength aluminium alloys, Nature. 549 (2017) 365–369. doi:10.1038/nature23894.
[9] J.R. Croteau, S. Griffiths, M.D. Rossell, C. Leinenbach, C. Kenel, V. Jansen, D.N. Seidman, D.C. Dunand, N.Q. Vo, Microstructure and mechanical properties of Al-Mg-Zr alloys processed by selective laser melting, Acta Mater. 153 (2018) 35–44. doi:10.1016/j.actamat.2018.04.053.
[10] F.F. Conde, J.D. Escobar, J.P. Oliveira, M. Béreš, A.L. Jardini, W.W. Bose, J.A. Avila, Effect of thermal cycling and aging stages on the microstructure and bending strength of a selective laser melted 300-grade maraging steel, Mater. Sci. Eng. A. (2019). doi:10.1016/j.msea.2019.03.129.
[11] O.O. Salman, C. Gammer, A.K. Chaubey, J. Eckert, S. Scudino, Effect of heat treatment on microstructure and mechanical properties of 316L steel synthesized by selective laser melting, Mater. Sci. Eng. A. 748 (2019) 205–212. doi:10.1016/j.msea.2019.01.110.
[12] K. Moussaoui, W. Rubio, M. Mousseigne, T. Sultan, F. Rezai, Effects of Selective Laser Melting additive manufacturing parameters of Inconel 718 on porosity, microstructure and mechanical properties, Mater. Sci. Eng. A. 735 (2018) 182–190. doi:10.1016/j.msea.2018.08.037.
[13] X. Li, J.J. Shi, C.H. Wang, G.H. Cao, A.M. Russell, Z.J. Zhou, C.P. Li, G.F. Chen, Effect of heat treatment on microstructure evolution of Inconel 718 alloy fabricated by selective laser melting, J. Alloys Compd. 764 (2018) 639–649. doi:10.1016/j.jallcom.2018.06.112.
[14] C.L. Yang, Z.J. Zhang, S.J. Li, Y.J. Liu, T.B. Sercombe, W.T. Hou, P. Zhang, Y.K. Zhu, Y.L. Hao, Z.F. Zhang, R. Yang, Simultaneous improvement in strength and plasticity of Ti-24Nb-4Zr-8Sn manufactured by selective laser melting, Mater. Des. 157 (2018) 52–59. doi:10.1016/j.matdes.2018.07.036.
[15] J. Stef, A. Poulon-Quintin, A. Redjaimia, J. Ghanbaja, O. Ferry, M. De Sousa, M. Gouné, Mechanism of porosity formation and influence on mechanical properties in selective laser melting of Ti-6Al-4V parts, Mater. Des. 156 (2018) 480–493. doi:10.1016/j.matdes.2018.06.049.
[16] C. Zhang, H. Zhu, H. Liao, Y. Cheng, Z. Hu, X. Zeng, Effect of heat treatments on fatigue property of selective laser melting AlSi10Mg, Int. J. Fatigue. 116 (2018) 513–522. doi:10.1016/j.ijfatigue.2018.07.016.

[17] I. Rosenthal, R. Shneck, A. Stern, Heat treatment effect on the mechanical properties and fracture mechanism in AlSi10Mg fabricated by additive manufacturing selective laser melting process, Mater. Sci. Eng. A. 729 (2018) 310–322. doi:10.1016/j.msea.2018.05.074.
[18] H. Zhang, H. Zhu, T. Qi, Z. Hu, X. Zeng, Selective laser melting of high strength Al-Cu-Mg alloys: Processing, microstructure and mechanical properties, Mater. Sci. Eng. A. 656 (2016) 47–54. doi:10.1016/j.msea.2015.12.101.
[19] X. Nie, H. Zhang, H. Zhu, Z. Hu, L. Ke, X. Zeng, Analysis of processing parameters and characteristics of selective laser melted high strength Al-Cu-Mg alloys: From single tracks to cubic samples, J. Mater. Process. Technol. 256 (2018) 69–77. doi:10.1016/j.jmatprotec.2018.01.030.
[20] Z. Hu, H. Zhang, H. Zhu, Z. Xiao, X. Nie, X. Zeng, Microstructure, mechanical properties and strengthening mechanisms of AlCu5MnCdVA aluminum alloy fabricated by selective laser melting, Mater. Sci. Eng. A. (2019). doi:10.1016/j.msea.2019.04.114.
[21] T. Qi, H. Zhu, H. Zhang, J. Yin, L. Ke, X. Zeng, Selective laser melting of Al7050 powder: Melting mode transition and comparison of the characteristics between the keyhole and conduction mode, Mater. Des. 135 (2017) 257–266. doi:10.1016/j.matdes.2017.09.014.
[22] P. Wang, H.C. Li, K.G. Prashanth, J. Eckert, S. Scudino, Selective laser melting of Al-Zn-Mg-Cu: Heat treatment, microstructure and mechanical properties, J. Alloys Compd. 707 (2017) 287–290. doi:10.1016/j.jallcom.2016.11.210.
[23] R. Xiao, X. Zhang, Problems and issues in laser beam welding of aluminum-lithium alloys, J. Manuf. Process. 16 (2014) 166–175. doi:10.1016/j.jmapro.2013.10.005.
[24] K. Wei, Z. Wang, X. Zeng, Preliminary investigation on selective laser melting of Ti-5Al-2.5Sn α-Ti alloy: From single tracks to bulk 3D components, J. Mater. Process. Technol. 244 (2017) 73–85. doi:10.1016/j.jmatprotec.2017.01.032.
[25] Z. Hu, H. Zhu, H. Zhang, X. Zeng, Experimental investigation on selective laser melting of 17-4PH stainless steel, Opt. Laser Technol. 87 (2017) 17–25. doi:10.1016/j.optlastec.2016.07.012.
[26] K.G. Prashanth, S. Scudino, T. Maity, J. Das, J. Eckert, Is the energy density a reliable parameter for materials synthesis by selective laser melting?, Mater. Res. Lett. 5 (2017) 386–390. doi:10.1080/21663831.2017.1299808.